

# PRODUCTION OF ALL THE $r$ -PROCESS NUCLIDES IN THE DYNAMICAL EJECTA OF NEUTRON STAR MERGERS

SHINYA WANAJO<sup>1</sup>, YUICHIRO SEKIGUCHI<sup>2</sup>, NOBUYA NISHIMURA<sup>3</sup>, KENTA KIUCHI<sup>2</sup>, KOUTAROU KYUTOKU<sup>4</sup>, AND MASARU SHIBATA<sup>2</sup>

*Draft version March 3, 2014*

## ABSTRACT

Recent studies suggest that binary neutron star (NS-NS) mergers robustly produce the heavy  $r$ -process nuclei above the atomic mass number of  $A \sim 130$  because of their ejecta consisting of almost pure neutrons (electron fraction of  $Y_e \ll 0.1$ ). This conflicts, however, with the so-called “universality” of the (solar-like)  $r$ -process pattern evidenced by spectroscopic analyses of Galactic halo stars. We present, for the first time, the result of nucleosynthesis calculations based on the fully general-relativistic simulation of a NS-NS merger with approximate neutrino transport. It is found that the bulk of the dynamical ejecta are appreciably shock-heated and neutrino-processed, resulting in a wide range of  $Y_e$  ( $\approx 0.09$ – $0.45$ ). The mass-averaged abundance distribution of calculated nucleosynthesis yields is in remarkable agreement with the full-mass range ( $A \approx 90$ – $240$ ) of the solar  $r$ -process curve. This implies, if our model is representative of such events, that the dynamical ejecta of NS-NS mergers can be the origin of the Galactic  $r$ -process nuclei. Our result also shows that the radioactive heating after  $\sim 1$  day from the merging, giving rise to  $r$ -process-powered transient emission, is dominated by the  $\beta$ -decays of several species close to stability with precisely measured half-lives. This implies that the total radioactive heating rate for such an event can be well constrained within about a factor of two if the ejected material has a solar-like  $r$ -process pattern.

*Subject headings:* nuclear reactions, nucleosynthesis, abundances — stars: abundances — stars: neutron

## 1. INTRODUCTION

The astrophysical site of the  $r$ -process, the rapid neutron-capture process that makes half the elements heavier than iron, remains a long-standing mystery of nucleosynthesis. Recently, compact binary mergers (CBMs) of double neutron star (NS-NS) and black hole–neutron star (BH-NS) systems have received considerable attention as possible sources of the  $r$ -process nuclei (Lattimer & Schramm 1974; Symbalisty & Schramm 1982; Eichler et al. 1989; Meyer 1989; Freiburghaus et al. 1999) according to the following reasons.

First, radioactively powered “kilonova” emission from the  $r$ -processed ejecta can be a promising electro-magnetic counterpart to the gravitational-wave signal from a CBM event (Li & Paczyński 1998; Metzger et al. 2010; Goriely et al. 2011; Kasen et al. 2013; Barnes & Kasen 2013; Tanaka & Hotokezaka 2013; Grossman et al. 2014). The possible identification of a kilonova associated with the *Swift* GRB 130603B (Berger et al. 2013; Tanvir et al. 2013) also indicates that CBMs are the progenitors of short-duration gamma-ray bursts and the sources of  $r$ -process elements (Hotokezaka et al. 2013a; Tanaka et al. 2014).

Another reason is that core-collapse supernovae (CC-SNe; in particular the proto-NS wind), the site that has been believed to be the promising sources

of the  $r$ -process nuclei, are found to provide only marginal conditions for making the elements beyond iron (e.g. Martínez-Pinedo et al. 2012; Roberts et al. 2012; Fischer et al. 2012). Detailed nucleosynthesis studies with such physical environments confirm that CCSNe produce the elements only up to the atomic mass number of  $A \sim 110$  (Wanajo et al. 2011; Wanajo 2013). One possible exception could be the scenario of (still hypothetical) rapidly rotating, strongly magnetized CCSN cores (Winteler et al. 2012).

Recently, Goriely et al. (2011) and Bauswein et al. (2013) have explored nucleosynthesis based on the approximate (conformally flat spatial metric) general-relativistic (GR) simulations of NS-NS mergers. They found that the ejecta had extremely low electron fractions ( $Y_e \ll 0.1$ ), leading to fission recycling and thus robust production of *only* heavy  $r$ -process nuclei with  $A \gtrsim 130$ . Similar results have been also obtained from the Newtonian simulations of NS-NS and BH-NS mergers by other groups (Roberts et al. 2011; Korobkin et al. 2012; Rosswog et al. 2014).

These nucleosynthetic results conflict, however, with the so-called “universality” of the  $r$ -process abundance pattern evidenced by recent spectroscopic studies of Galactic halo stars (e.g. Sneden et al. 2008). That is, all  $r$ -process-enhanced stars exhibit atmospheric abundance distributions that closely follow the solar  $r$ -process abundance pattern for the atomic number  $Z \gtrsim 38$  ( $A \gtrsim 90$ ), in particular for  $Z \gtrsim 56$  ( $A \gtrsim 140$ ). There has been no sign of nucleosynthetic events making the nuclei exclusively with  $A > 130$ .

In this Letter, we report our first result of nucleosynthesis study based on the full-GR, approximate neutrino transport simulation of a NS-NS merger. The GR effects,

<sup>1</sup> National Astronomical Observatory of Japan, 2-21-1 Osawa, Mitaka, Tokyo 181-8588, Japan; shinya.wanajo@nao.ac.jp

<sup>2</sup> Yukawa Institute for Theoretical Physics, Kyoto University, Kyoto 606-8502, Japan

<sup>3</sup> Astrophysics, EPSAM, Keele University, Keele, ST5 5BG, UK

<sup>4</sup> Department of Physics, University of Wisconsin-Milwaukee, P.O. Box 413, Milwaukee, WI 53201, USA

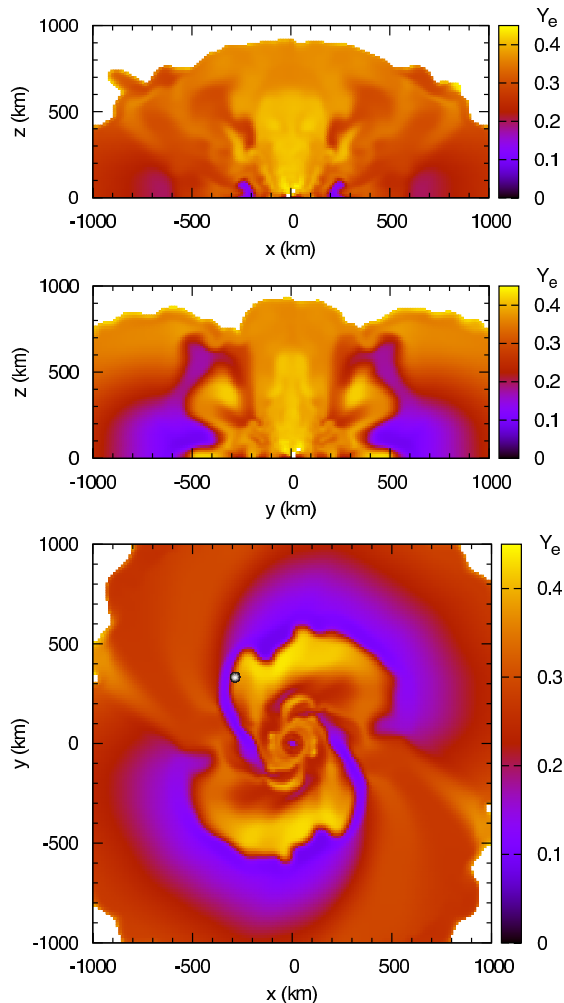


FIG. 1.— Color-coded  $Y_e$  distributions on the  $x$ - $z$  (top),  $y$ - $z$  (middle), and  $x$ - $y$  (bottom; orbital) planes at the end of simulation (13.7 ms after the merging). The open circle on the orbital plane indicates one of the representative tracer particles (see text).

being crucial for the dynamical evolutions of merger ejecta (Hotokezaka et al. 2013b), were not fully taken into account in the previous studies. Moreover, neutrino effects that can affect the ejecta  $Y_e$  are neglected in all previous studies. Our NS-NS merger model is described in Section 2. The subsequent nucleosynthesis result is presented in Section 3. The radioactive heating rates (relevant for kilonova emission) are also obtained from the nucleosynthesis calculations (Section 4).

## 2. MERGER MODEL

The hydrodynamical evolution of a NS-NS merger is followed with a recently-developed 3D full-GR code (Y. Sekiguchi et al. 2014, in preparation), which is updated from the previous version (Sekiguchi 2010; Sekiguchi et al. 2011a,b). Neutrino transport is taken into account based on the Thorne’s moment scheme (Thorne 1981; Shibata et al. 2011) with a closure relation. For neutrino heating, absorption on free nucleons is considered. The gravitational masses (in isolation) are taken to be  $1.3 M_\odot$  for both NSs.

We adopt an equation of state (EOS) of dense matter developed in Steiner et al. (2013, SFXo), which has the maximum NS mass sufficiently greater than the

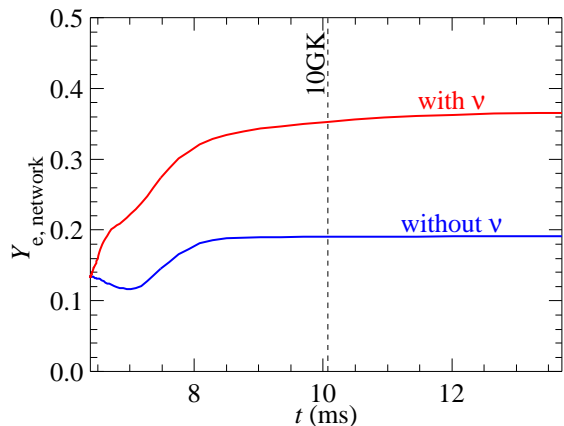


FIG. 2.— Temporal evolution of  $Y_{e,\text{network}}$  for a selected tracer particle from  $t = 6.39$  ms to 13.7 ms, which is re-computed by the reaction network in post-processing steps. The red and blue lines indicate the evolutions with and without the neutrino captures on free nucleons, respectively. The dashed line marks the time when the temperature decreases to 10 GK.

largest well-measured mass ( $\approx 2 M_\odot$ , Demorest et al. 2010; Antoniadis et al. 2013). This EOS gives the radius of  $\approx 12$  km for a cold NS, being in the middle of the range constrained from nuclear experiments, nuclear theory, and astrophysical observations, 10.7–13.1 km for a  $1.4 M_\odot$  NS (Lattimer & Lim 2013). Note that the EOS of Shen et al. (1998) adopted in many previous simulations gives  $\approx 14.5$  km for a  $1.4 M_\odot$  NS, being substantially greater than the upper bound of this constraint.

The simulation ends at the time  $t = 13.7$  ms after the onset of merger. At this time, the bulk of ejecta (total mass of  $M_{\text{ej}} \approx 0.01 M_\odot$ ) are freely expanding with the velocities of  $\sim (0.1\text{--}0.3)c$  ( $c$  is the speed of light). The ejecta expand, not only along the orbital plane (as seen in the Newtonian simulations of Korobkin et al. 2012; Rosswog et al. 2014), but toward the non-orbital directions (Figure 1; also in the GR simulations of Hotokezaka et al. 2013b; Bauswein et al. 2013). This is due to compact NSs in GR gravity as well as the small NS radius from the Steiner’s EOS. The resulting strong gravity enhances powerful shock formation at their contact surface region. Consequently, the ejecta expand toward all directions, making a hot envelope surrounding the newly formed hyper-massive NS (HMNS). Spiral arms are also formed along the orbital plane.

The temperatures near the HMNS surface get as high as  $\sim 10$  MeV ( $\sim 100$  GK), giving rise to copious  $e^-e^+$  pairs that activate the four weak interactions,  $n + e^+ \rightarrow \bar{\nu}_e + p$ ,  $p + e^- \rightarrow \nu_e + n$ , and their inverses. Thus,  $e^+$  and  $\nu_e$  captures convert some part of neutrons to protons; the ejecta  $Y_e$ ’s increase from the initially low values ( $\ll 0.1$ ). The first outgoing, spiral-arm shaped ejecta ( $\sim 500\text{--}700$  km at the end of simulation; Figure 1, bottom) are away from the HMNS when it forms and thus the neutrino effects are unimportant. As a result, the  $Y_e$ ’s are relatively low ( $\sim 0.1\text{--}0.2$ ). The outer diluted envelope with relatively high  $Y_e$  ( $\sim 0.2\text{--}0.3$ ; outside of the arms in purple) is subdominant in the total ejecta mass.

The mass ejection continues in response to the interaction between the inner envelope and the rapidly rotating, quasi-radially oscillating HMNS (Hotokezaka et al. 2013b). This can be seen in Figure 1 (bottom) as the structured spiral arms in the range  $\lesssim 500$  km. In this

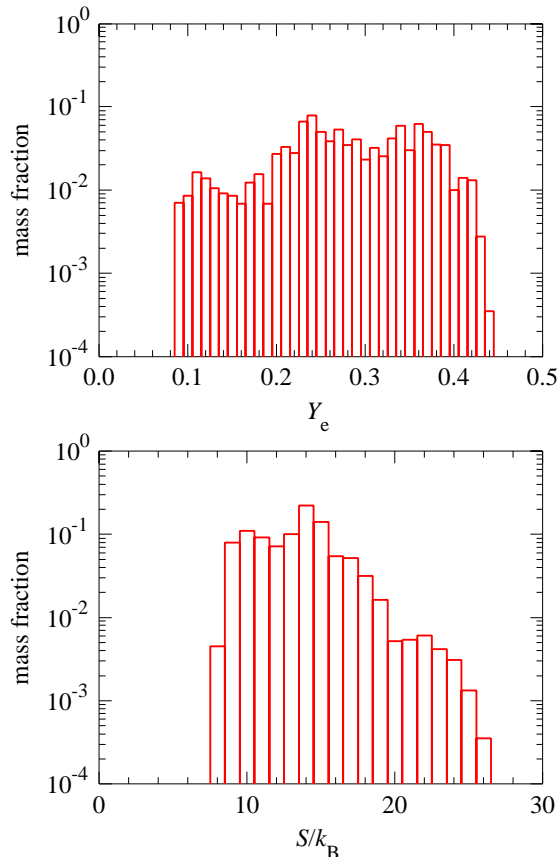


FIG. 3.— Ejecta mass fractions vs.  $Y_e$  (top) and  $S/k_B$  (bottom) at the end of simulation. The widths of  $Y_e$  and  $S/k_B$  are chosen to be  $\Delta Y_e = 0.01$  and  $\Delta S/k_B = 1$ , respectively.

phase, neutrinos coming from the HMNS surface play a crucial role and the  $Y_e$ 's become  $\sim 0.2$ – $0.4$ . Bipolar structures as found in Hotokezaka et al. (2013b), with  $Y_e \sim 0.4$ , can also be seen in Figure 1 (top and middle panels).

To make clear the role of neutrinos, the  $Y_e$  evolution is re-computed by the reaction network ( $Y_{e,\text{network}}$ ) for a selected Lagrangian mass-element particle (an open circle in Figure 1, bottom) traced from our grid-based simulation. The computation is initiated at  $t = 6.39$  ms with the simulation value of  $Y_e = 0.134$  when the temperature is still high ( $\sim 50$  GK). The  $Y_{e,\text{network}}$  from this time to  $t = 13.7$  ms (the end of simulation;  $\sim 6$  GK) is followed by the network with the thermodynamic quantities of the tracer particle. The temporal neutrino luminosities and mean energies are adopted as those angle averaged from the simulation result. Figure 2 displays the resulting  $Y_{e,\text{network}}$  evolutions with (red) and without (blue) the neutrino captures on free nucleons. We find that, without the neutrino captures, the  $Y_{e,\text{network}}$  still increases by positron capture but only to 0.19 at  $t = 13.7$  ms. With the neutrino captures, in contrast, the  $Y_{e,\text{network}}$  reaches 0.37 at  $t = 13.7$  ms (which is in agreement with the simulation  $Y_e$ ).

The ejecta mass fractions of  $Y_e$ 's (top) and entropies (per nucleon;  $S/k_B$ ,  $k_B$  is Boltzmann's constant, bottom) at the end of simulation evaluated on the orbital plane are displayed in Figure 3 with the widths of  $\Delta Y_e = 0.01$  and  $\Delta S/k_B = 1$ , respectively. We find that the  $Y_e$ 's widely distribute between 0.09 and 0.45 with greater

amounts for higher  $Y_e$ , in which the initial  $\beta$ -equilibrium values ( $\ll 0.1$ ) have gone. Strong shock heating and also (to lesser extent) neutrino heating result in  $S/k_B = 8$ – $26$  (with generally higher values for higher  $Y_e$ ), being sizably greater than those in the previous studies ( $S/k_B \sim 1$ – $3$ , Goriely et al. 2011).

### 3. THE $r$ -PROCESS

The nucleosynthesis analysis makes use of the thermodynamic trajectories of the ejecta particles traced on the orbital plane. A representative particle is chosen from each  $Y_e$ -bin (from  $Y_e = 0.09$  to  $0.44$  with the interval of  $\Delta Y_e = 0.01$ ) shown in Figure 3 (top). For simplicity, we do not analyze the non-orbital components because of the dominance of the ejecta masses close to the orbital plane. Each nucleosynthesis calculation is initiated when the temperature decreases to 10 GK, where the initial composition is given by  $Y_e$  and  $1 - Y_e$  for the mass fractions of free protons and neutrons, respectively.

The reaction network consists of 6300 species, all the way from single neutrons and protons to the  $Z = 110$  isotopes relevant for the  $r$ -process. Experimental rates, when available, are taken from the latest versions of REACLIB<sup>5</sup> (Cyburt et al. 2010) and Nuclear Wallet Cards<sup>6</sup>. Otherwise, the theoretical estimates of fusion rates<sup>7</sup> (TALYS, Goriely et al. 2008) and  $\beta$ -decay half-lives (GT2, Tachibana et al. 1990) are adopted, where both are based on the same nuclear mass model (HFB-21, Goriely et al. 2010). Theoretical fission properties adopted are those estimated on the basis of the HFB-14 mass model (Goriely et al. 2009). For fission fragments, a Gaussian-type distribution (Kodama & Takahashi 1975) is assumed with emission of four prompt neutrons per event (Goriely et al. 2013). Neutrino captures are not included, which make only slight shifts of  $Y_e$  (typically an increase of  $\sim 0.01$  from 10 GK to 5 GK; see Figure 2).

The hydrodynamical trajectories end with the temperatures of  $\sim 5$  GK. Further temporal evolutions are followed by the density drop like  $t^{-3}$  and with the temperatures computed with the EOS of Timmes & Swesty (2000) by adding the entropies generated by  $\beta$ -decay, fission, and  $\alpha$ -decay. This entropy generation slows the temperature drop around 1 GK (see, e.g., Korobkin et al. 2012). The effect is, however, less dramatic than those found in the previous works because of the higher ejecta entropies in our result.

Figure 4 (top) displays the final nuclear abundances for selected trajectories. We find a variety of nucleosynthetic outcomes: iron-peak and  $A \sim 90$  abundances made in nuclear quasi-equilibrium for  $Y_e \gtrsim 0.4$ , light  $r$ -process abundances for  $Y_e \sim 0.2$ – $0.4$ , and heavy  $r$ -process abundances for  $Y_e \lesssim 0.2$ . Different from the previous works, we find no fission recycling; the nuclear flow for the lowest  $Y_e$  ( $= 0.09$ ) trajectory reaches  $A \sim 280$ , the fissile point by neutron-induced fission, only at the freezeout of  $r$ -processing. Spontaneous fission plays an important role for forming the  $A \sim 130$  abundance peak, but only for  $Y_e < 0.15$ .

Figure 4 (bottom) shows the mass-averaged nuclear

<sup>5</sup> <https://groups.nsl.msu.edu/jina/reactlib/db/index.php>.

<sup>6</sup> <http://www.nndc.bnl.gov/wallet/>

<sup>7</sup> <http://www.astro.ulb.ac.be/pmwiki/Brusslib/Brusslib>.

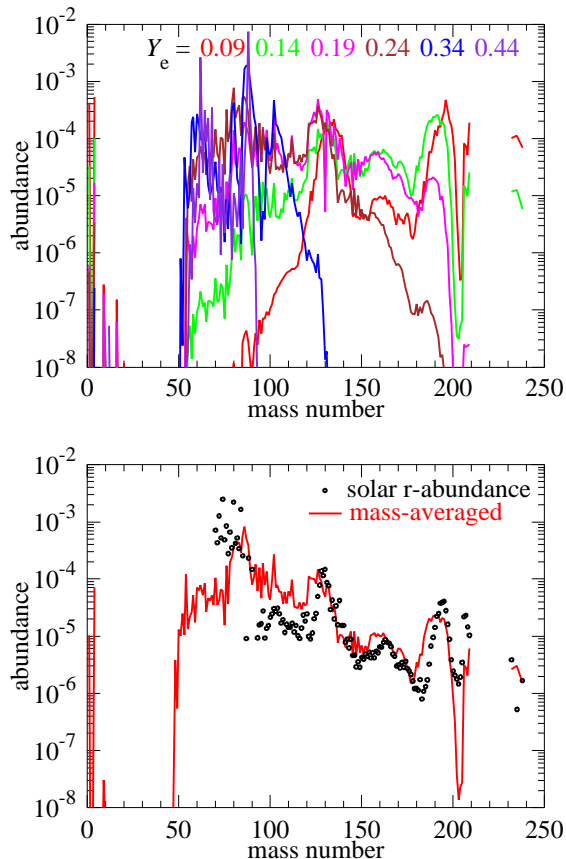


FIG. 4.— Final nuclear abundances for selected trajectories (top;  $Y_e = 0.09, 0.14, 0.19, 0.24, 0.34$ , and  $0.44$ ) and that mass-averaged (bottom; compared with the solar  $r$ -process abundances).

abundances by weighting the final yields for the representative trajectories with their  $Y_e$  mass fractions (Figure 3). We find a remarkable agreement of our result with the solar  $r$ -process abundance distribution over the full- $A$  range of  $\sim 90$ –240. This striking result, differing from the previous works exhibiting production of  $A > 130$  nuclei only, is a consequence of the wide  $Y_e$  distribution predicted from our full-GR merger simulation with neutrino effects taken into account. Note also that fission plays only a subdominant role for the final nucleosynthetic abundances. The second ( $A \sim 130$ ) and rare-earth-element ( $A \sim 160$ ) peak abundances are dominated by direct production from the trajectories of  $Y_e \sim 0.2$ . Our result reasonably reproduces the solar-like abundance ratio between the second ( $A \sim 130$ ) and third ( $A \sim 195$ ) peaks as well, which is difficult to explain by fission recycling.

Given that the model is representative of NS-NS mergers, our result gives an important implication; the dynamical component of NS-NS merger ejecta can be the dominant origin of the Galactic  $r$ -process nuclei. Other contributions from, e.g., the BH-torus wind after collapse of HMNSs (Surman et al. 2008; Wanajo & Janka 2012; Fernández & Metzger 2013), as invoked in the previous studies to account for the (solar-like)  $r$ -process universality, may not be needed. The amount of the entirely  $r$ -processed ejecta,  $M_{\text{ej}} \approx 0.01 M_{\odot}$ , with present estimates of the Galactic event rate, a few  $10^{-5} \text{ yr}^{-1}$  (e.g., Dominik et al. 2012), is also compatible with

the mass of the Galactic  $r$ -process abundances (e.g., Wanajo & Janka 2012).

#### 4. RADIOACTIVE HEATING

The  $r$ -processing ends a few 100 ms after the onset of merger. The subsequent abundance changes by  $\beta$ -decay, fission, and  $\alpha$ -decay are followed up to 100 days after the merging; the resulting radioactive heating is relevant for kilonova emission. Figure 5 displays the temporal evolutions of the heating rates for selected trajectories (top-left) and those mass-averaged (top-right). For a comparison purpose, the heating rate for the nuclear abundances with the solar  $r$ -process pattern ( $\dot{q}_{\text{solar-}r}$ ),  $\beta$ -decaying back from the initial composition at neutron-separation energies of 2 MeV ( $A \geq 90$ , the same as that used in Hotokezaka et al. 2013a; Tanaka et al. 2014), is also shown by a black-solid line in each panel. The short-dashed line indicates an analytical approximation defined by  $\dot{q}_{\text{analytic}} \equiv 2 \times 10^{10} t^{-1.3}$  (in units of  $\text{erg g}^{-1} \text{ s}^{-1}$ ;  $t$  is time in day, see, e.g., Metzger et al. 2010). Lower panels are the same as the upper panels, but for those relative to  $\dot{q}_{\text{analytic}}$ .

Overall, each curve reasonably follows  $\dot{q}_{\text{analytic}}$  by  $\sim 1$  day. After this time, the heating is dominated by a few radioactivities and becomes highly dependent on  $Y_e$ . Contributions from the ejecta of  $Y_e > 0.3$  are generally unimportant after  $\sim 1$  day. We find that the heating for  $Y_e = 0.34$  turns to be significant after a few 10 days because of the  $\beta$ -decays from  $^{85}\text{Kr}$  (half-life of  $T_{1/2} = 10.8 \text{ yr}$ ; see Figure 4, bottom, for its large abundance),  $^{89}\text{Sr}$  ( $T_{1/2} = 50.5 \text{ d}$ ), and  $^{103}\text{Ru}$  ( $T_{1/2} = 39.2 \text{ d}$ ). Heating rates for  $Y_e = 0.19$  and  $0.24$ , whose abundances are dominated by the second peak nuclei, are found to be in good agreement with  $\dot{q}_{\text{solar-}r}$ . This is due to a predominance of  $\beta$ -decay heating from the second peak abundances, e.g.,  $^{123}\text{Sn}$  ( $T_{1/2} = 129 \text{ d}$ ) and  $^{125}\text{Sn}$  ( $T_{1/2} = 9.64 \text{ d}$ ) around a few 10 days.

Our result shows that the heating rate for the lowest  $Y_e$  ( $= 0.09$ ) is the greatest after 1 day (Figure 5, left panels). The values are larger than the previous results (with  $Y_e \sim 0.02$ – $0.04$  in Goriely et al. 2011; Rosswog et al. 2014) by a factor of a few. In our case, the radioactive heating is dominated by the spontaneous fissions of  $^{254}\text{Cf}$ ,  $^{259}\text{Fm}$  and  $^{262}\text{Fm}$ . It should be noted, however, the heating from spontaneous fission is highly uncertain because of the many unknown half-lives and decay modes of nuclides reaching to this quasi-stable region ( $A \sim 250$ – $260$  with  $T_{1/2}$  of days to years). In fact, tests with another set of theoretical estimates show a few times smaller rates after  $\sim 1$  day (as a result of diminishing contributions from  $^{259}\text{Fm}$  and  $^{262}\text{Fm}$ ), being similar to the previous works. It appears, therefore, difficult to obtain reliable heating rates with currently available nuclear data when fission plays a dominant role.

In our result the total heating rate is dominated by  $\beta$ -decays all the times (Figure 5, right panels) because of the small ejecta amount of  $Y_e < 0.15$  (in which fission becomes important). The radioactive heating after  $\sim 1$  day is mostly due to the  $\beta$ -decays from a small number of species with precisely measured half-lives. Uncertainties in nuclear data are thus irrelevant. The mass-averaged heating rate for  $t \sim 1$ – $10$  days is smaller than  $\dot{q}_{\text{analytic}}$  and  $\dot{q}_{\text{solar-}r}$  because of the overabundances near



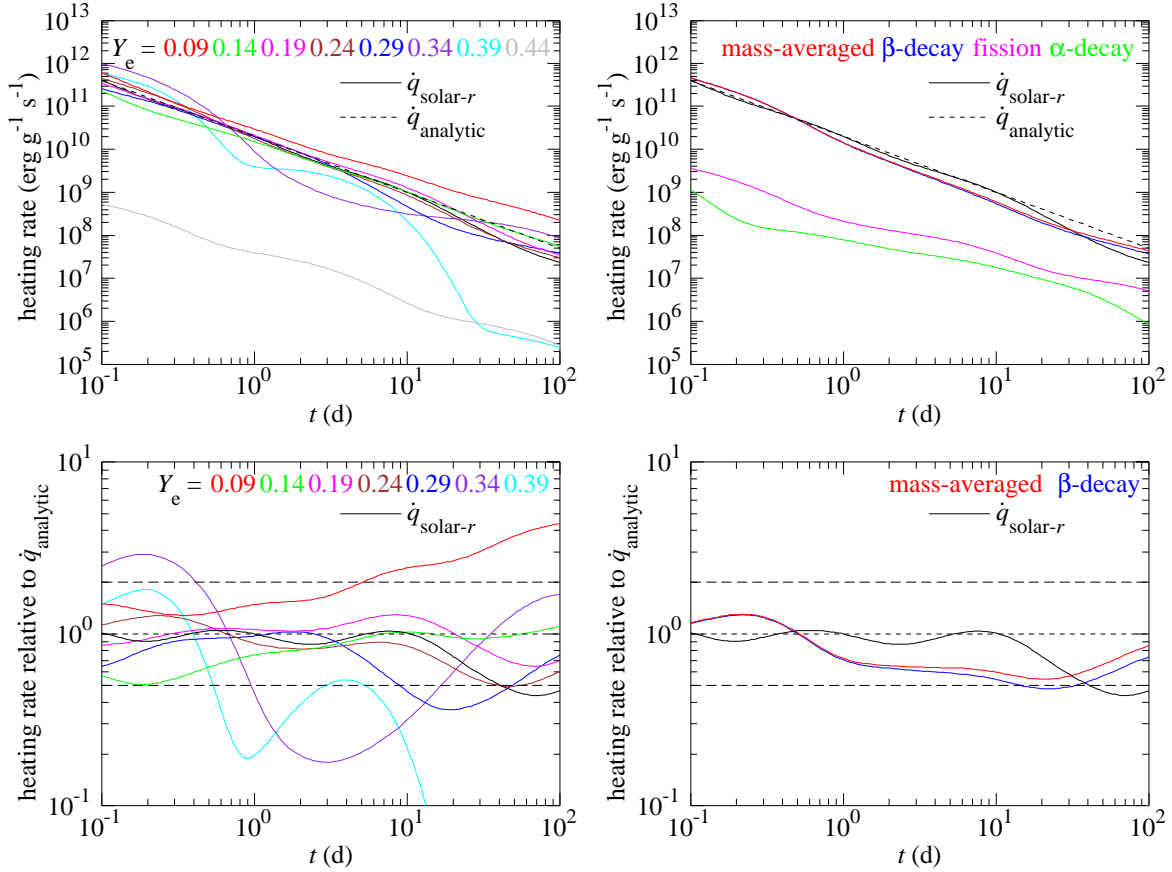


FIG. 5.— Heating rates as functions of  $t$  (days after the merging) for selected trajectories (top-left;  $Y_e = 0.09, 0.14, 0.19, 0.24, 0.29, 0.34, 0.39$ , and  $0.44$ ) and those mass-averaged (top-right; also shown are those from  $\beta$ -decay, fission, and  $\alpha$ -decay). In each panel, the heating rates for the solar  $r$ -process pattern ( $\dot{q}_{\text{solar-}r}$ ; see text) and the analytical approximation  $\dot{q}_{\text{analytic}} = 2 \times 10^{10} t^{-1.3}$  (erg g $^{-1}$  s $^{-1}$ ) are shown by black-solid and short-dashed lines, respectively. Lower panels are the same as the upper panels but for those relative to  $\dot{q}_{\text{analytic}}$ . Long-dashed lines indicate the factor of 2 ranges from unity (short-dashed line).

$A = 100$  (Figure 4, bottom) that do not significantly contribute to radioactive heating. The differences are, however, still within about a factor of two. In conclusion, if merger ejecta have a solar  $r$ -process-like abundance pattern,  $\dot{q}_{\text{solar-}r}$  (and  $\dot{q}_{\text{analytic}}$ ) can be a reasonable approximation for kilonova emission<sup>8</sup>.

It is important to note that our merger simulation exhibits different  $Y_e$  distributions between the orbital and polar directions (Figure 1). Multi-dimensional information of nucleosynthetic abundances will be needed when we discuss the angular dependences of kilonova emission (Roberts et al. 2011; Grossman et al. 2014).

## 5. SUMMARY

We examined  $r$ -process calculations based on the full-GR, approximate neutrino transport simulation of the NS-NS merger with the equal masses ( $= 1.3 M_\odot$ ) of NSs. Different from previous studies, the merger ejecta exhibited a wide range of  $Y_e \sim 0.1\text{--}0.4$  that led to the nucleosynthetic abundance distribution being in excellent agreement with the solar  $r$ -process pattern. Given that the model is representative, our result (with the present

estimate of the Galactic event rate) implies that NS-NS mergers can be the major origin of the  $r$ -process elements in the Galaxy.

Our result also indicates that the radioactive heating (that powers a kilonova transient) after  $\sim 1$  day from the onset of merger is dominated by the  $\beta$ -decays of a small number of species with measured half-lives. The total heating rates are thus well approximated by the  $\beta$ -decays of the solar  $r$ -process-like abundances as well as by the approximation of  $\propto t^{-1.3}$ . Detailed multi-dimensional information of nucleosynthesis abundances should be, however, taken into account when we consider the spatial dependences of kilonova emission.

Our result implies that the previous thought of NS-NS merger events, dynamically ejecting almost pure NS matter, should be reconsidered. The shock-heated and neutrino-processed ejecta from a HMNS are in fact modestly neutron-rich: the phenomenon that is similar to the early stage of a CCSN (a proto-NS instead of a HMNS). Much more works will be, however, needed to test if similar results are obtained with different NS masses and their ratios, with other (reasonable) EOSs, with higher spatial resolution, etc. Nucleosynthetic contributions from BH-NS mergers, as well as from the BH-accretion tori subsequent to NS-NS/BH-NS mergers, should be also explored to draw conclusions on the role of CBMs to the Galactic chemical evolution of the  $r$ -process nuclei.

<sup>8</sup> These heating rates correspond to the heating efficiency, defined by  $f \equiv \dot{Q} t_{\text{peak}} / M_{\text{ej}} c^2$  ( $\dot{Q}$  and  $t_{\text{peak}}$  are the total heating rate and the peak time of a kilonova transient, Li & Paczyński 1998), of  $f/10^{-6} \approx 1$  and  $0.5$  for  $t_{\text{peak}} = 1$  and  $10$  days, respectively, with the thermalization factor of  $0.5$  (Metzger et al. 2010).

We are grateful to S. Goriely and T. Tachibana for providing the data of fission properties and theoretical  $\beta$ -decay rates. The project was supported by the JSPS Grants-in-Aid for Scientific Research (23224004, 23740160, 24244028, 24740163, 25103510, 25103512, 25105508), Grant-in-Aid for Scientific Research on Innovative Area (20105004), and EU-FP7-ERC-2012-St Grant 306901. Koutarou Kyutoku is supported by JSPS

Postdoctoral Fellowships for Research Abroad. CBM simulations were in part performed on Cray XC30 at CfCA of NAOJ and Fujitsu FX10 at (Information Technology Center of) the University of Tokyo. This work was in part developed during the long-term workshop on Gravitational Waves and Numerical Relativity held at the Yukawa Institute for Theoretical Physics, Kyoto University in May and June 2013.

## REFERENCES

- Antoniadis, J., Freire, P. C. C., Wex, N., et al. 2013, *Sci*, 340, 6131  
 Barnes, J., & Kasen, D. 2013, *ApJ*, 775, 18  
 Bauswein, A., Goriely, S., & Janka, H.-T. 2013, *ApJ*, 773, 78  
 Berger, E., Fong, W., & Chornock, R. 2013, *ApJL*, 774, L23  
 Cyburt, R. H., Amthor, A. M., Ferguson, R., et al. 2010, *ApJS*, 189, 240  
 Demorest, P. B., Pennucci, R., Ransom, S. M., Roberts, M. S. E., & Hessels, J. W. T. 2010, *Natur*, 467, 1081  
 Dominik, M., Belczynski, K., Fryer, C., et al. 2012, *ApJ*, 759, 52  
 Eichler, D., Livio, M., Piran, T., & Schramm, D. N. 1989, *Natur*, 340, 126  
 Fernández, R., & Metzger, B. D. 2013, *MNRAS*, 435, 502  
 Fischer, T., Martínez-Pinedo, G., Hempel, M., & Liebendörfer, M. 2012, *PhRvD*, 85, 083003  
 Freiburghaus, C., Rosswog, S., & Thielemann, F.-K. 1999, *ApJL*, 525, L121  
 Goriely, S., Hilaire, S., & Koning, A. J. 2008, *A&A*, 487, 767  
 Goriely, S., Hilaire, S., Koning, A. J., Sin, M., & Capote, R. 2009, *PhRvC*, 79, 024612  
 Goriely, S., Chamel, N., & Pearson, J. M. 2010, *PhRvC*, 82, 035804  
 Goriely, S., Chamel, N., Janka, H.-T., & Pearson, J. M. 2011, *A&A*, 531, A78  
 Goriely, S., Sida, J.-L., Lemaître, J.-F., et al. 2013, *PhRvL*, 111, 242502  
 Grossman, D., Korobkin, O., Rosswog, S., & Piran, T. 2014, *arXiv:1307.2943*  
 Hotokezaka, K., Kyutoku, K., Tanaka, M., et al. 2013, *ApJL*, 778, L16  
 Hotokezaka, K., Kiuchi, K., Kyutoku, K., et al. 2013, *PhRvD*, 87, 024001  
 Kasen, D., Badnell, N. R., & Barnes, J. 2013, *ApJ*, 774, 25  
 Kodama, T., & Takahashi, K. 1975, *Nucl. Phys. A*, 239, 489  
 Korobkin, O., Rosswog, S., Arcones, A., & Winteler, C. 2012, *MNRAS*, 426, 1940  
 Lattimer, J. M., & Schramm, D. N. 1974, *ApJ*, 192, L145  
 Lattimer, J. M., & Lim, Y. 2013, *ApJ*, 771, 51  
 Li, L.-X., & Paczyński, B. 1998, *ApJ*, 507, L59  
 Martínez-Pinedo, G., Fischer, T., Lohs, A., & Huther, L. 2012, *PhRvL*, 109, 251104  
 Metzger, B. D., Martínez-Pinedo, G., Darbha, S., et al. 2010, *MNRAS*, 406, 2650  
 Meyer, B. S. 1989, *ApJ*, 343, 254  
 Roberts, L. F., Kasen, D., Lee, W. H., & Ramirez-Ruiz, E. 2011, *ApJL*, 736, L21  
 Roberts, L. F., Reddy, S., & Shen, G. 2012, *PhRvC*, 86, 065803  
 Rosswog, S., Korobkin, O., Arcones, A., & Thielemann, F.-K. 2014, *arXiv:1307.2939*  
 Sekiguchi, Y. 2010, *Prog. Theor. Phys.*, 124, 331  
 Sekiguchi, Y., Kiuchi, K., Kyutoku, K., & Shibata, M. 2011, *PhRvL*, 107, 051102  
 Sekiguchi, Y., Kiuchi, K., Kyutoku, K., & Shibata, M. 2011, *PhRvL*, 107, 211101  
 Shen, H., Toki, H., Oyamatsu, K., & Sumiyoshi, K. 1998, *Nucl. Phys. A*, 637, 435  
 Shibata, M., Kiuchi, K., Sekiguchi, Y., & Suwa, Y. 2011, *Prog. Theor. Phys.*, 125, 1255  
 Sneden, C., Cowan, J. J., & Gallino, R. 2008, *ARA&A*, 46, 241  
 Steiner, A. W., Lattimer, J. M., & Brown, E. F. 2013, *ApJL*, 765, L5  
 Symbalist, E., & Schramm, D. N. 1982, *ApL*, 22, 143  
 Surman, R., McLaughlin, G. C., Ruffert, M., Janka, H.-Th., & Hix, W. R. 2008, *ApJ*, 679, L117  
 Tachibana, T., Yamada, M., & Yoshida, Y. 1990, *PThPh*, 84, 641  
 Tanaka, M., & Hotokezaka, K. 2013, *ApJ*, 775, 113  
 Tanaka, M., Hotokezaka, K., Kyutoku, K., et al. 2014, *ApJ*, 780, 31  
 Tanvir, N. R., Levan, A. J., Fruchter, A. S., et al. 2013, *Natur*, 500, 547  
 Timmes, F. X., & Swesty, F. D. 2000, *ApJS*, 126, 501  
 Thorne, K. S. 1981, *MNRAS*, 194, 439  
 Wanajo, S., Janka, H.-T., & Müller, B. 2011, *ApJL*, 726, L15  
 Wanajo, S., & Janka, H.-T. 2012, *ApJ*, 746, 180  
 Wanajo, S. 2013, *ApJL*, 770, L22  
 Winteler, C., Käppeli, R., Perego, A., et al. 2012, *ApJL*, 750, L22